Heterogeneous Catalysis Hot Paper

DOI: 10.1002/anie.201407140

Geometry-Assisted Three-Dimensional Superlocalization Imaging of Single-Molecule Catalysis on Modular Multilayer Nanocatalysts**

Rui Han, Ji Won Ha, Chaoxian Xiao, Yuchen Pei, Zhiyuan Qi, Bin Dong, Nicholas L. Bormann, Wenyu Huang, and Ning Fang**

Abstract: *To establish the structure–catalytic property relationships of heterogeneous catalysts, a detailed characterization of the three-dimensional (3D) distribution of active sites on a single catalyst is essential. Single-particle catalysis of a modular multilayer catalytic platform that consists of a solid silica core, a mesoporous silica shell, and uniformly distributed Pt nanoparticles sandwiched in between these layers is presented. The first 3D high-resolution super-localization imaging of single fluorescent molecules produced at active sites on the core-shell model nanocatalysts is demonstrated. The 3D mapping is aided by the well-defined geometry and a correlation study in scanning electron microscopy and total internal reflection fluorescence and scattering microscopy. This approach can be generalized to study other nano- and mesoscale structures.*

Heterogeneous catalysis has been studied extensively by various surface science techniques on single-crystal surfaces.[1–3] Much understanding has been achieved about the structure of active sites and the catalytic reaction mechanisms. However, most catalysts used in industry are metal nanoparticles (NPs) supported on three-dimensional (3D) porous supports.[4–6] The techniques that can be used to understand the distribution of active sites on these 3D supports are very limited, especially if the characterization has to be carried out under reaction conditions.

High-resolution electron tomography is the most broadly used technique in measuring the distribution of metal NPs in 3D supports. For example, within individual zeolite Y particles, the numbers, size distributions, and interparticle distances of Pt particles have been characterized.[7] The heterogeneities of Pt loading in the zeolite were discovered to vary up to a factor of 35 between different zeolite crystals, which clearly demonstrated the importance of catalyst preparation and characterization. Electron tomography was also able to measure the location and size distribution of Pd NPs on and inside carbon nanotubes of different internal diameters.[8]

Recent developments of in situ transmission electron microscopy (TEM) have opened up exciting new opportunities to acquire fundamental understanding of reaction mechanisms of heterogeneous catalysis.[9,10] However, its applicability is still greatly limited by technical challenges, such as the use of sophisticated sample holders, strict restrictions on experimental conditions, inability to capture chemical information of reagents and products, and relatively slow speed to carry out tomography scans.

To study the activity, selectivity, and mechanism of action of single nanocatalysts under real-life conditions, single-molecule super-localization fluorescence microscopy has been employed to map individual fluorogenic turnover events on single nanocatalysts with nanoscale localization precision in the two-dimensional (2D) horizontal plane.[11–23] This fluorescence super-resolution mapping technique is advantageous over other spectroscopic techniques, such as electrochemical detection[24] and surface plasmon spectroscopy,[25,26] for acquiring detailed information on single nanocatalysts. Recent investigations have led to better understanding of the effects of facets,[11,27] defects,[16] and photogenerated reactive sites (electrons and holes)[17] in single nanocatalysts. Furthermore, 3D super-resolution imaging has been demonstrated by stochastic optical reconstruction microscopy (STORM) for determining both axial and lateral positions of individual fluorophores in cells.[28,29] However, the 3D super-resolution mapping on single nanocatalysts under reaction conditions has not been reported so far, and it is still elusive because the axial localization precision[30] (typically 2–3 times the corresponding lateral localization precision) is often insufficient to resolve the axial distribution of fluorescent events on single nanocatalysts of up to a few hundred nanometers high.

Herein, we report the first 3D super-resolution mapping of catalytic activities in a model multilayer catalytic platform under reaction conditions. This model platform (Figure 1 A), which consists of Pt NPs sandwiched between an optically transparent solid SiO_2 core (ca. 200 nm in diameter) and a mesoporous SiO_2 shell (SiO_2@Pt@mSiO_2),[31] resembles the

[*] Dr. R. Han,[+] Dr. J. W. Ha,[+] Dr. C. Xiao, Y. Pei, Z. Qi, B. Dong, N. L. Bormann, Prof. Dr. W. Huang, Prof. Dr. N. Fang
Ames Laboratory, U.S. Department of Energy, and Department of Chemistry, Iowa State University
Ames, Iowa, 50011 (USA)
E-mail: whuang@iastate.edu
nfang@iastate.edu
Dr. J. W. Ha[+]
Department of Chemistry, Northwestern University
2145 Sheridan Road, Evanston, Illinois 60208 (USA)

[+] These authors contributed equally to this work.

[**] This work was supported by U.S. Department of Energy, Office of Basic Energy Sciences, Chemical Sciences, Geosciences, and Biosciences Division (instrument development) and by the Laboratory Directed Research and Development (LDRD) program of the Ames Laboratory (catalysis, platform synthesis). W.H. also thanks Iowa State University and the Ames Laboratory (Royalty Account) for startup funds. The Ames Laboratory is operated for the U.S. Department of Energy by Iowa State University under contract no. DE-AC02-07CH11358.

Supporting information for this article is available on the WWW under http://dx.doi.org/10.1002/anie.201407140.

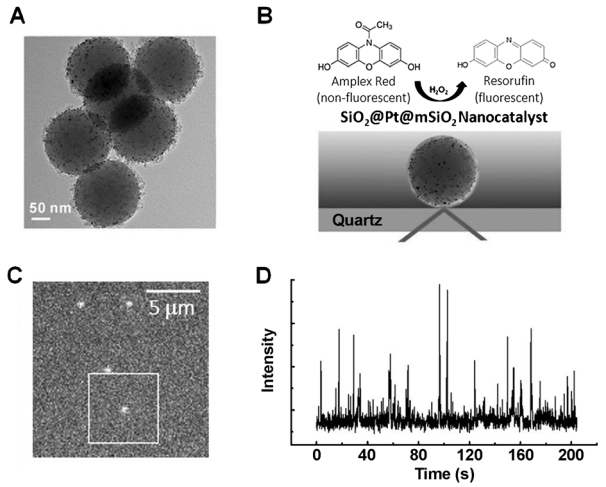

Figure 1. Single-molecule catalysis of a fluorogenic oxidation reaction on single SiO_2@Pt@mSiO_2 nanocatalysts. A) TEM image of Pt NPs confined between a SiO_2 sphere and a mesoporous SiO_2 shell. B) Experiment using total internal reflection fluorescence microscopy. Non-fluorescent amplex red is converted into highly fluorescent resorufin by a SiO_2@Pt@mSiO_2 nanocatalyst in the presence of H_2O_2. C) Typical image of fluorescent product at localized spots during the catalytic reaction under 532 nm illumination. D) A typical plot of fluorescence intensity vs. time for the fluorescent spot highlighted in the white frame in (C). Temporal resolution was 100 ms. The corresponding movie is included as Movie S1 in the Supporting Information.

nanostructures of many intensively investigated high-performance core–shell nanocatalysts.[32–39]

This type of multilayer nanocatalyst is an attractive heterogeneous model catalyst for the following reasons: First, the catalytic activity can be tuned readily by controlling the number of the supported metal NPs. Second, the outer SiO_2 mesoporous shells isolate the catalytically active metal NPs and protect them from the possibility of sintering during catalytic reactions at high temperatures, while allowing reactant molecules to approach the surface of metal NPs through the pores. Third, spherical nanocatalysts can be employed as a 3D multilayer catalytic platform for systematic investigations to understand the factors (such as size, structure, molecular transport) affecting their catalytic properties and efficiency. There have been no reports to study the catalytic behavior of this type of multilayer nanocatalysts at the single-molecule and single-particle levels under turnover conditions. In this context, it is highly desirable to go beyond the averaging inherent in ensemble experiments and reveal catalytic properties of individual nanocatalysts during catalytic reactions.

The multilayer SiO_2@Pt@mSiO_2 nanocatalysts used in this study were synthesized according to literature procedures (see details in the Supporting Information, Figure S1).[31] As shown in Figure 1 A, the Pt NPs with a diameter of 3.6 ± 0.7 nm are sandwiched between a SiO_2 sphere with an average diameter of 200 ± 20 nm and a SiO_2 shell with an average thickness of about 10 nm. SiO_2 was chosen as both core and shell material because it has excellent thermal stability, tunable surface functionality, and optical transparency in the UV/Vis range. The UV/Vis absorption spectra of the multilayer nanocatalysts and the SiO_2 spheres are shown in the Supporting Information, Figure S2; a peak is observed at around 275 nm in Figure S2 A because of the presence of Pt NPs.[40]

To investigate the catalytic activity of the multilayer nanocatalysts, we used the fluorogenic oxidation reaction of non-fluorescent amplex red (10-acetyl-3,7-dihydroxyphenoxazine) to produce highly fluorescent resorufin ($\lambda_{ex} = 563$ nm; $\lambda_{em} = 587$ nm, at pH 7.5) at the single-molecule level (Figure 1 B).[17] A sample slide was prepared by spin-casting the nanocatalyst solution on a poly-L-lysine functionalized fused quartz slide. The concentration of the nanocatalysts immobilized on the fused quartz slide was controlled to be about 1 μm^{-2} for single-particle catalysis. Two pieces of double-sided tape with a thickness of 25 μm were used as spacer between the fused quartz slide and a glass coverslip to form a sample flow chamber.

Single molecule imaging experiments were carried out under a prism-type total internal reflection (TIR) fluorescence microscope (Supporting Information, Figure S3).[41] An evanescent field is created when the total internal reflection of an incident laser beam occurs at the solid/liquid interface. The evanescent field intensity decays exponentially with the vertical distance (up to a few hundred nanometers) from the interface.[42] This unique home-built prism-type TIR fluorescence microscope is capable of finding the optimum incident angle automatically by scanning a range of angles at intervals as small as 0.2°.[41] The optimum incident angle in our experiments was found to be about 68°, which was close to the critical angle of 66° for the fused quartz/water interface, to result in a deep penetration depth and the highest possible signal-to-noise ratio (S/N) for single molecule detection.

A 532 nm green laser was used to excite the fluorescent resorufin product. Before initiating the fluorogenic oxidation reaction, the 532 nm laser beam was first shined onto the sample for 20 min to remove possible fluorescent dusts and impurities. Then the reactant-containing solution (0.4 μM amplex red, 20 mM H_2O_2, and 50 mM pH 7.5 phosphate buffer) was introduced over the nanocatalysts in the sample flow chamber. Pt NPs are very reactive in the fluorogenic oxidation reaction of amplex red to resorufin.[14] Thus, fluorescent resorufin molecules were formed at many possible reactive Pt NPs on single nanocatalysts (Figure 1 C; Supporting Information, S4A) and detected by an electron multiplying charge-coupled device (EMCCD) camera. These experiments clearly demonstrated the nanocatalyst activity for the fluorogenic reaction at the single-particle level.

We recorded movies of stochastic fluorescence bursts at many localized spots on the fused quartz surface with a temporal resolution of 100 ms. Figure 1 D shows a segment of a typical fluorescence intensity trajectory from one spot highlighted in the white frame in Figure 1 C containing stochastic fluorescence ON–OFF signals. Each burst corresponds to a single resorufin molecule. It is evident in Figure 1 D that these fluorescence bursts vary significantly in intensity with the S/N ranging from 3 to 12. This can be ascribed primarily to different vertical positions of these resorufin molecules on the surface of a 200 nm spherical

nanocatalyst within the evanescent field, which extends only a few hundred nanometers into the sample.

The fluorescence image of a single resorufin molecule during one burst spreads over a few pixels as a point spread function (PSF; Supporting Information, Figure S4A). The center position of this PSF can be determined by 2D Gaussian fitting of its fluorescence profile (Figure S4B). The localization precision is typically in the range of a few nanometers to tens of nanometers depending on the signal to noise ratios (S/N) of individual fluorescence bursts. Furthermore, to correct for sample drifting, two red-fluorescent beads with a diameter of 100 nm were used as position marker (Figures S4A and S5).

This commonly used localization method generates high-resolution 2D maps of individual turnover events on single nanocatalysts; however, it does not provide essential information related to the nanocatalyst 3D structure. To surmount this limitation, we have made further efforts to develop a new approach for geometry-assisted 3D superlocalization imaging of single fluorescent molecules in the evanescent field. The core idea is to take advantage of the uniform spherical shape of the nanocatalysts. The new approach consists of two key steps. First, the Pythagoras theorem is used to convert 2D to 3D localization of each resorufin molecule on the nanocatalyst spherical surface. Second, the volume intensity is used to determine whether a given product molecule is formed at the top or bottom half of a spherical nanocatalyst (see the detailed procedure in the Supporting Information, Figure S6).

Two sets of experiments have been performed to validate the method described above. The first set verifies that the intrinsic fluctuations in the molecular fluorescence emission do not significantly affect the accuracy in the vertical position determination. We plotted (Supporting Information, Figure S7) the S/N distributions of resorufin molecules immobilized on a flat surface or produced catalytically on the spherical surface of the nanocatalysts under similar experimental conditions. The relative standard deviation (RSD) of the S/N distribution for the spherical surface case (ca. 36%) is significantly larger than that for the flat surface case (ca. 9%). The vertical distribution of resorufin molecules in the evanescent field is the main cause of this disparity, and it is also the more significant factor contributing to the recorded fluorescence intensity variations than the intrinsic fluctuations. Furthermore, it should be emphasized that the fluorescence intensity is only used to determine on which hemisphere a resorufin molecule is located, and this operation can tolerate much larger uncertainties in the fluorescence intensity than those caused by the intrinsic fluctuations.

Another relevant point of discussion on uncertainty is about the resorufin molecules located in the middle section (equator) of a spherical nanocatalyst. These molecules have to be treated as one group because of the lack of resolving power to decide whether they are actually above or below the equator. The width of this middle section is estimated to be roughly ± 10 nm when the RSD of the fluorescence intensity fluctuations is set to 10%. The complete analysis at different incident angles and intensity fluctuations can be found in the Supporting Information.

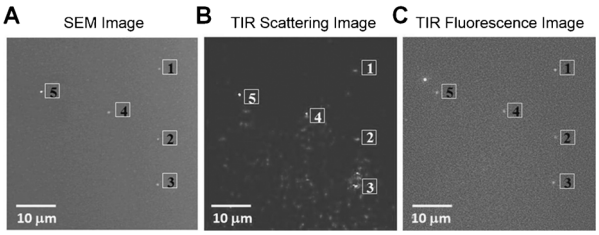

Figure 2. Correlation of SEM (A), TIR scattering (B), and TIR fluorescence (C) images of the same area showing five single SiO2@Pt@m-SiO2 nanocatalysts (high Pt NP loading).

The second set of experiments was a correlation study of same nanocatalysts in scanning electron microscopy (SEM), TIR scattering microscopy, and TIR fluorescence microscopy (Figure 2). The position and diameter of each nanocatalyst were first measured in the SEM image (Figure 2A). Then we located the same nanocatalysts in the TIR scattering mode, which was converted from the TIR fluorescence mode by simply replacing the 532 nm long-pass filter for fluorescence emission with a 532 nm band-pass filter for laser excitation in front of the EMCCD camera. The 2D Gaussian fitting method was used again here to determine the center position of each nanocatalyst in the TIR scattering image (Figure 2B). Finally, we performed the fluorogenic oxidation reaction over the same nanocatalyst sample as described earlier, and recorded a series of movies showing stochastic fluorescence bursts in the same sample area. All five nanocatalysts labeled in Figure 2 were active for the catalytic reaction, as the corresponding fluorescence bursts were found in the correlated TIR fluorescence image (Figure 2C). A MATLAB program was developed to carry out the data analysis for the entire imaging area (Supporting Information, Figure S8). Through the careful correlation study, 3D super-resolution maps of resorufin molecules on single nanocatalysts can be generated reliably and accurately.

Figure 3 shows the 3D super-resolution map of single resorufin product molecules formed on NP4 during the catalytic reactions. The diameter of NP4 was measured to be 240 nm from the high-magnification SEM image (Figure 3A). As expected for this nanocatalyst with a high density of Pt NPs, a large number of turnover events were recorded within about 1 h. Figure 3B shows a broad distribution of the signal intensity, which is consistent with the intensity trajectory provided in Figure 1D. In the 2D super-resolution map (Figure 3C), a circular shape can be observed with an estimated diameter of 270 nm, which is consistent with the particle diameter of 240 nm plus the uncertainties in 2D localization. The center of the circle nearly overlaps with the geometric center of the nanocatalyst obtained from the correlated TIR scattering image (Figure 2B). Finally, the 2D coordinates of the resorufin molecules were projected onto the spherical surface to generate the final 3D super-resolution map (Figure 3D).

To further demonstrate the 3D super-resolution mapping, we synthesized similar nanocatalysts but with a very low density of Pt NPs (1–5 Pt NPs per particle) (Figure 4A). We performed the same fluorogenic reaction over the low Pt loading nanocatalysts under identical experimental condi-

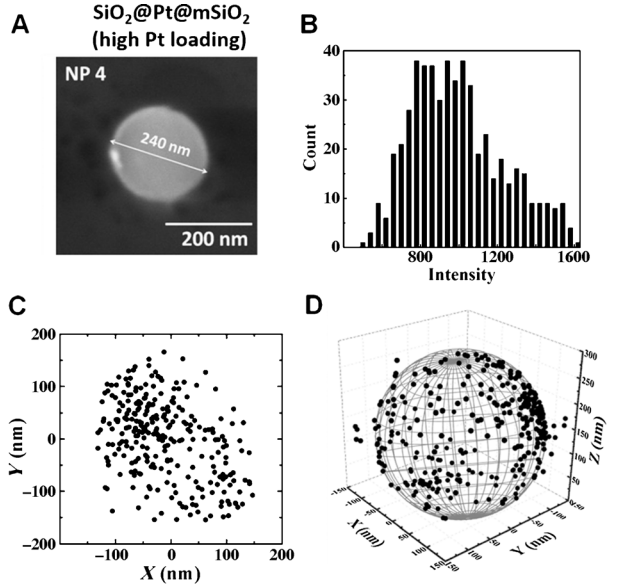

Figure 3. 3D super-localization imaging on a high Pt loading nanocatalyst. This particle is labeled as NP4 in Figure 2. A) High-magnification SEM image. B) A broad fluorescence intensity distribution obtained from all of the fluorescent molecules produced during a catalytic reaction. C) 2D super-resolution map of single product molecules. The geometric center of the nanocatalyst measured from the TIR scattering image is set to (0,0). D) 3D super-resolution map.

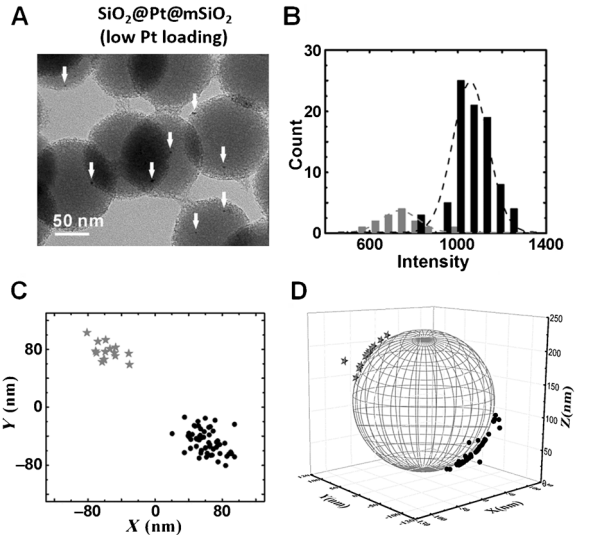

Figure 4. 3D super-localization imaging on the low Pt loading SiO_2@Pt@$mSiO_2$ nanocatalysts. A) TEM image of the nanocatalysts. The Pt NPs are indicated by the white arrows. B) Two groups of fluorescence intensity distribution. C) 2D super-resolution map showing two separate groups on the nanocatalyst. D) 3D super-resolution map. The nanocatalyst diameter was estimated from the TEM image.

tions. As shown in Figure 4B, we found two distributions of fluorescence intensity of single product molecules on a nanocatalyst.

Figure 4C shows a 2D super-resolution map of single product molecules. Two groups of the turnover events can be observed on the 2D map. It can be found from the two intensity distributions (Figure 4B) that one group (black dots with higher fluorescence intensity) is positioned at the lower side of this nanocatalyst while the other group (gray stars with lower fluorescence intensity) is located at the upper side. The observation of the two intensity groups serves as further evidence that the fluorescence intensity can be used as the secondary criterion together with the primary criterion (2D location) to assign individual fluorescence bursts to the 3D spherical surface. It can also be observed in Figure 4B that the shoulders of the two distributions overlap owing to the intrinsic fluorescence fluctuations, causing common and expected uncertainty associated with single molecule imaging experiments.

Another example with three groups of localized fluorescence bursts is provided in the Supporting Information, Figure S9. These two examples clearly demonstrate the capability to conduct the 3D super-resolution mapping of single fluorescent molecules produced on a 3D nanocatalyst.

In conclusion, we report the first 3D super-resolution mapping of single fluorescent product molecules on single spherical multilayer nanocatalysts during catalytic oxidation reactions. The 3D imaging is aided by the well-defined geometry of the nanocatalyst, a careful correlation study in SEM and TIR scattering and fluorescence microscopy, and an algorithm to convert 2D maps to 3D maps. This super-resolution mapping approach can be generalized to study other regularly shaped nano- and mesoscale structures, if the actual shapes and dimensions can be established through correlated SEM or TEM images.

Single molecule catalysis with 3D super-localization imaging allowed us to better understand the catalytic activity, the identity and 3D distribution of reactive sites of the multilayer nanocatalysts. Note that the SiO_2@Pt@$mSiO_2$ nanocatalysts are a highly modular 3D multilayer catalytic platform with controllable pore size, length, and active site location. We therefore expect that the sandwiched core–shell catalytic platform combined with the 3D super-localization imaging technique will enable us to address more fundamental challenges such as molecular transport phenomena in the porous catalytic nanostructures. Further studies to clarify the catalytic efficiency and characteristic molecular transport phenomena in terms of the thickness of a shell and the size of pores in the highly modular catalytic platform are underway.

Received: July 12, 2014
Revised: August 17, 2014
Published online: September 26, 2014

Keywords: heterogeneous catalysis · mesoporous silica · multilayer nanocatalysts · platinum · three-dimensional imaging

[1] J. W. A. Sachtler, G. A. Somorjai, *J. Catal.* **1983**, *81*, 77–94.
[2] F. Zaera, G. A. Somorjai, *J. Am. Chem. Soc.* **1984**, *106*, 2288–2293.
[3] P. S. Cremer, X. C. Su, Y. R. Shen, G. A. Somorjai, *J. Am. Chem. Soc.* **1996**, *118*, 2942–2949.
[4] A. Iglesias-Juez, A. M. Beale, K. Maaijen, T. C. Weng, P. Glatzel, B. M. Weckhuysen, *J. Catal.* **2010**, *276*, 268–279.

[5] B. Barghi, M. Fattahi, F. Khorasheh, *React. Kinet. Mech. Catal.* **2012**, *107*, 141 – 155.
[6] K. Thavornprasert, B. d. L. G. d. Menorval, M. Capron, J. Gornay, L. Jalowiecki-Duhamel, X. Secordel, S. Cristol, J. L. Dubois, F. Dumeignil, *Biofuels* **2012**, *3*, 25 – 34.
[7] J. Zečević, A. M. J. van der Eerden, H. Friedrich, P. E. de Jongh, K. P. de Jong, *ACS Nano* **2013**, *7*, 3698 – 3705.
[8] O. Ersen, J. Werckmann, M. Houllé, M.-J. Ledoux, C. Pham-Huu, *Nano Lett.* **2007**, *7*, 1898 – 1907.
[9] A. R. Harutyunyan, G. Chen, T. M. Paronyan, E. M. Pigos, O. A. Kuznetsov, K. Hewaparakrama, S. M. Kim, D. Zakharov, E. A. Stach, G. U. Sumanasekera, *Science* **2009**, *326*, 116 – 120.
[10] H. Yoshida, Y. Kuwauchi, J. R. Jinschek, K. Sun, S. Tanaka, M. Kohyama, S. Shimada, M. Haruta, S. Takeda, *Science* **2012**, *335*, 317 – 319.
[11] M. B. J. Roeffaers, B. F. Sels, H. Uji-i, F. C. De Schryver, P. A. Jacobs, D. E. De Vos, J. Hofkens, *Nature* **2006**, *439*, 572 – 575.
[12] G. De Cremer, B. F. Sels, D. E. De Vos, J. Hofkens, M. B. J. Roeffaers, *Chem. Soc. Rev.* **2010**, *39*, 4703 – 4717.
[13] P. Chen, X. Zhou, H. Shen, N. M. Andoy, E. Choudhary, K.-S. Han, G. Liu, W. Meng, *Chem. Soc. Rev.* **2010**, *39*, 4560 – 4570.
[14] K. S. Han, G. Liu, X. Zhou, R. E. Medina, P. Chen, *Nano Lett.* **2012**, *12*, 1253 – 1259.
[15] W. Xu, P. K. Jain, B. J. Beberwyck, A. P. Alivisatos, *J. Am. Chem. Soc.* **2012**, *134*, 3946 – 3949.
[16] X. Zhou, N. M. Andoy, G. Liu, E. Choudhary, K.-S. Han, H. Shen, P. Chen, *Nat. Nanotechnol.* **2012**, *7*, 237 – 241.
[17] J. W. Ha, T. P. A. Ruberu, R. Han, B. Dong, J. Vela, N. Fang, *J. Am. Chem. Soc.* **2014**, *136*, 1398 – 1408.
[18] T. Tachikawa, T. Yonezawa, T. Majima, *ACS Nano* **2013**, *7*, 263 – 275.
[19] M. B. J. Roeffaers, G. De Cremer, J. Libeert, R. Ameloot, P. Dedecker, A.-J. Bons, M. Bückins, J. A. Martens, B. F. Sels, D. E. De Vos, J. Hofkens, *Angew. Chem. Int. Ed.* **2009**, *48*, 9285 – 9289; *Angew. Chem.* **2009**, *121*, 9449 – 9453.
[20] S. A. Blum, *Phys. Chem. Chem. Phys.* **2014**, *16*, 16333.
[21] N. M. Andoy, X. Zhou, E. Choudhary, H. Shen, G. Liu, P. Chen, *J. Am. Chem. Soc.* **2013**, *135*, 1845 – 1852.
[22] W. Xu, H. Shen, Y. J. Kim, X. Zhou, G. Liu, J. Park, P. Chen, *Nano Lett.* **2009**, *9*, 3968 – 3973.
[23] X. Zhou, E. Choudhary, N. M. Andoy, N. Zou, P. Chen, *ACS Catal.* **2013**, *3*, 1448 – 1453.
[24] X. Xiao, S. Pan, J. S. Jang, F.-R. F. Fan, A. J. Bard, *J. Phys. Chem. C* **2009**, *113*, 14978 – 14982.
[25] C. Novo, A. M. Funston, P. Mulvaney, *Nat. Nanotechnol.* **2008**, *3*, 598 – 602.
[26] M. L. Tang, N. Liu, J. A. Dionne, A. P. Alivisatos, *J. Am. Chem. Soc.* **2011**, *133*, 13220 – 13223.
[27] T. Tachikawa, S. Yamashita, T. Majima, *J. Am. Chem. Soc.* **2011**, *133*, 7197 – 7204.
[28] B. Huang, W. Wang, M. Bates, X. Zhuang, *Science* **2008**, *319*, 810 – 813.
[29] S. A. Jones, S.-H. Shim, J. He, X. Zhuang, *Nat. Methods* **2011**, *8*, 499 – 505.
[30] H. Deschout, F. C. Zanacchi, M. Mlodzianoski, A. Diaspro, J. Bewersdorf, S. T. Hess, K. Braeckmans, *Nat. Methods* **2014**, *11*, 253 – 266.
[31] C. Xiao, R. V. Maligal-Ganesh, T. Li, Z. Qi, Z. Guo, K. T. Brashler, S. Goes, X. Li, T. W. Goh, R. E. Winans, W. Huang, *ChemSusChem* **2013**, *6*, 1915 – 1922.
[32] Y. Deng, Y. Cai, Z. Sun, J. Liu, C. Liu, J. Wei, W. Li, C. Liu, Y. Wang, D. Zhao, *J. Am. Chem. Soc.* **2010**, *132*, 8466 – 8473.
[33] Y. Xu, J. Ma, Y. Xu, L. Xu, L. Xu, H. Li, H. Li, *RSC Adv.* **2013**, *3*, 851 – 858.
[34] A. C. S. Sekhar, C. J. Meera, K. V. Ziyad, C. S. Gopinath, C. P. Vinod, *Catal. Sci. Technol.* **2013**, *3*, 1190 – 1193.
[35] S. H. Joo, J. Y. Park, C.-K. Tsung, Y. Yamada, P. Yang, G. A. Somorjai, *Nat. Mater.* **2009**, *8*, 126 – 131.
[36] J.-N. Park, A. J. Forman, W. Tang, J. Cheng, Y.-S. Hu, H. Lin, E. W. McFarland, *Small* **2008**, *4*, 1694 – 1697.
[37] H. Yang, Y. Chong, X. Li, H. Ge, W. Fan, J. Wang, *J. Mater. Chem.* **2012**, *22*, 9069 – 9076.
[38] J. Ge, Q. Zhang, T. Zhang, Y. Yin, *Angew. Chem. Int. Ed.* **2008**, *47*, 8924 – 8928; *Angew. Chem.* **2008**, *120*, 9056 – 9060.
[39] Z. Ma, S. Dai, *ACS Catal.* **2011**, *1*, 805 – 818.
[40] S. Afolake, M. van Jacqueline, G. W. Chris, *Nanotechnology* **2012**, *23*, 035102.
[41] W. Sun, K. Marchuk, G. F. Wang, N. Fang, *Anal. Chem.* **2010**, *82*, 2441 – 2447.
[42] D. Axelrod in *Biophysical Tools for Biologists, Volume Two: In Vivo Techniques*, *Vol. 89*, 1edst ed(Eds.: J. J. Correia, H. W. Detrich), Academic Press, New York, **2008**, pp. 169 – 221.

